Elsevier Editorial System(tm) for Chemical Engineering Journal

Manuscript Draft

Manuscript Number:

Title: Mimics of microstructures of Ni substituted Mn1-xNixCo2O4 for high energy density asymmetric capacitors

Article Type: Research Paper

Section/Category: Materials Synthesis and Processing

Keywords: Mixed transition metal oxides, Nanostructures, Asymmetric capacitor

Corresponding Author: Dr. Deepak Dubal, M.Sc.Ph.D.

Corresponding Author's Institution: Catalan Institute of Nanoescience and Nanotechnology

First Author: Mohaseen Tamboli

Order of Authors: Mohaseen Tamboli; Deepak Dubal, M.Sc.Ph.D.; Santosh Patil; Asiya Shaikh; Virendra Deonikar; Milind Kulkarni; Noormahamad Maldar; Pedro Gomez-Romero; Bharat Kale; Deepak Patil

Abstract: The preparation of nanostructured hierarchical MnxNi1-xCo2O4 metal oxides as efficient supercapacitors of different structures and configurations especially for the miniaturized electronics is still a challenge. In this context, we report template free facile hydrothermal synthesis of hierarchical nanostructured MnxNi1-xCo2O4 with excellent supercapacitive performance. Significantly, the morphology of pure MnCo2O4 transformed from 3D microcubes to 1D nanowires with incorporation of Ni. The electrochemical study shows highest specific capacity i.e. 734 C/g for Mn0.4Ni0.6Co2O4 with high cycling stability of 89.2 % which is much higher than pristine MnCo2O4 and NiCo2O4. Later, asymmetric capacitor has been fabricated successfully using Mn0.4Ni0.6Co2O4 nanowires as positive electrode and activated carbon (AC) as negative electrode in a KOH aqueous electrolyte. An asymmetric cell could be cycled reversibly in the high-voltage range of 0 to 1.5 V and displays intriguing performances with a specific capacitance of 112.8 F/g (6.87 F/cm3) and high energy density of 35.2 Wh/kg (2.1 mWh/cm3). Importantly, this asymmetric capacitor device exhibits an excellent long cycle life along with 83.2 % specific capacitance retained after 2000 cycles.

Suggested Reviewers: babasaheb Sankapal
Applied Physics, Visvesvaraya National Institute of Technology, Nagpur
brsankapal@gmail.com
Expert in Chemical synthesis and supercapacitors

Surendra Shinde
Biological and Environmental Science, Dongguk University, South Korea
shindesurendra9@gmail.com
Expert in chemical synthesis of different nanomaterials for supercapacitor application

Yuping Wu Professor
chemistry, Fudan University, China
wuyp@fudan.edu.cn
Expert in various nanomaterials for energy storage applications such as Li-ion battery, supercapacitors

Rahul Salunkhe
chemistry, Natioanl Institute of Materials Science, Japan
salunkhe2002@gmail.com
Expert in Nickel cobalt oxide based materials, asymmetric supercapacitors

Opposed Reviewers:

Date: 26 June, 2016

To,

The Editor,

Chemical Engineering Journal

Dear Editor,

Attached please find an electronic version of the manuscript titled **"Mimics of microstructures of Ni substituted $Mn_{1-x}Ni_xCo_2O_4$ for high energy density asymmetric capacitors"** by Mohaseen S. Tamboli and Deepak P. Dubal *et al*. for your consideration for possible publication in ***Chemical Engineering Journal.***

In recent years many efforts are being made to discover new materials and fabricate new supercapacitors with increased energy densities. The mixed transition metal oxides (MTMOs), especially ternary metal oxides with two different metal ions, have received an upsurge interest as a promising supercapacitive electrode material. Important properties of the spinel structures depend crucially on the exact nature of the cation distribution over the octahedral and tetrahedral sites in the spinel cubic lattice. Moreover, the coupling of multiple metal species could render the MTMOs with rich redox reactions and improved electronic conductivity, which are beneficial to electrochemical applications. Among the various MTMOs, $MnCo_2O_4$ is one of the most promising candidates which has multiple valence states however the electrical conductivity of $MnCo_2O_4$ is too low, which limits its application in supercapacitors. On the other hand, $NiCo_2O_4$ possesses much better electronic conductivity and higher electrochemical activity than other MTMOs. In present investigation, we have tuned chemical compositions through substitution of Mn by Ni in $MnCo_2O_4$ which greatly enhances the electronic conductivity as well as electrochemical activity. In this respect, mixed manganese cobalt oxides with various compositions of Mn and Ni, other than $MnCo_2O_4$ can be anticipated with great potential for electrochemical energy storage.

In addition, asymmetric capacitor has been fabricated successfully using $Mn_{0.4}Ni_{0.6}Co_2O_4$ nanowires as positive electrode and activated carbon (AC) as negative electrode in a KOH aqueous electrolyte. An asymmetric cell could be cycled reversibly in the high-voltage range of 0 to 1.5 V and displays intriguing performances with a specific capacitance of 112.8 F/g (6.87 F/cm^3) and high energy density of 35.2 Wh/kg (2.1 mWh/cm^3). Importantly, this asymmetric capacitor device exhibits an excellent long cycle life along with 83.2 % specific capacitance retained after 2000 cycles.

These significant results reported are original and not published elsewhere. We believe this work fit well within the scope of ***Chemical Engineering Journal***. We will highly appreciate if you can consider

the above work for publication in the journal of ***Chemical Engineering Journal.***
Looking forward to hear positive response.

Yours sincerely,

Dr. Deepak P. Dubal, Ph. D.
Marie-Curie Fellow (BP-DGR), (Alexander von Humboldt Fellow, Germany)
Catalan Institute of Nanoscience and Nanotechnology, CIN2, ICN2 (CSIC-ICN)
Campus UAB, E-08193 Bellaterra (Barcelona), Spain

***List of Suggested Reviewers**

1) Dr. Babasaheb Sankapal
   Associate Professor
   Nano Materials and Device Laboratory, Applied Physics Department,
   Visvesvaraya National Institute of Technology, South Ambhazari Road
   Nagpur-440 010 (M.S.) India
   Email: brsankapal@gmail.com

2) Dr. Surendra Shinde
   Assistant Professor,
   Department of Biological and Environmental Science,
   Dongguk University, South Korea
   Email: shindesurendra9@gmail.com

3) Prof. Yuping Wu
   Professor, Cochair of IUPAC International Conference on Novel Materials and their Synthesis (NMS)
   Vice Dean, College of Energy Nanjing Tech University Nanjing 211816 China
   New Energy and Materials Laboratory (NEML) Department of Chemistry Fudan University Shanghai 200433 China
   Email: wuyp@fudan.edu.cn

4) Dr. Rahul Salunkhe
   National Institute for Materials Science (NIMS),
   Tsukuba, Japan
   Email: salunkhe2002@gmail.com

Mimics of microstructures of Ni substituted $Mn_{1-x}Ni_xCo_2O_4$ for high energy density asymmetric capacitors

Graphical abstract:

The transformation of 3D microstructures of $MnCo_2O_4$ into 1D nanowires by incorporation of Ni into Mn site has been demonstrated. Asymmetric capacitor has been fabricated using $Mn_{0.4}Ni_{0.6}Co_2O_4$ nanowires as positive electrode and activated carbon (AC) as negative electrode.

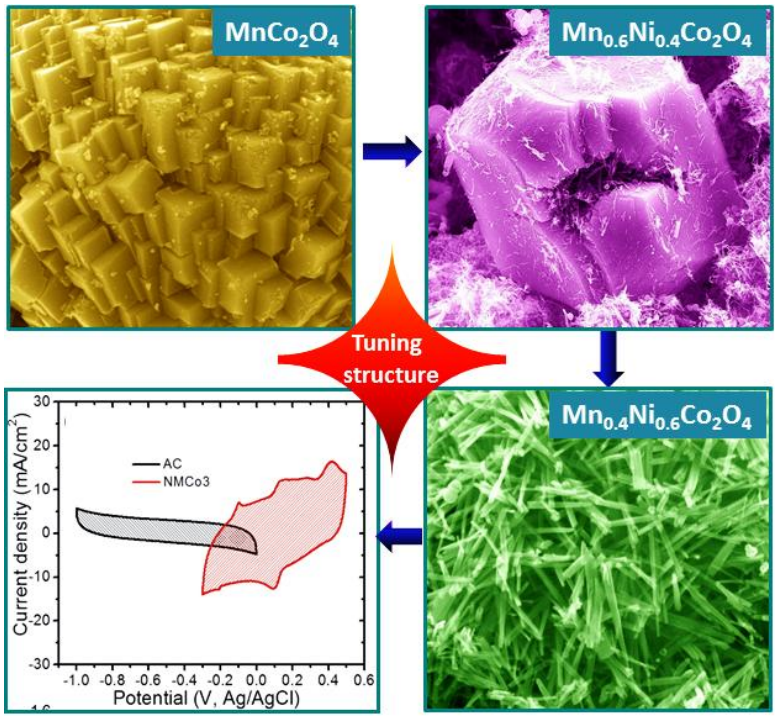

Research Highlights

- Hydrothermal synthesis of hierarchical $Mn_xNi_{1-x}Co_2O_4$ nanostructures
- Morphological transformation from 3D microcubes to 1D nanowires
- Fabrication of Asymmetric capacitor with activated carbon
- Excellent energy density (35.2 Wh/kg (2.1 mWh/cm^3))

Mimics of microstructures of Ni substituted $Mn_{1-x}Ni_xCo_2O_4$ for high energy density asymmetric capacitors

Mohaseen S. Tamboli[a,†], Deepak P. Dubal[c†], Santosh S. Patil[a], Asiya Shaikh[b], Virendra Deonikar[b], Milind V. Kulkarni[b], Noormahamad N. Maldar[b], Pedro Gomez-Romero[c,] Bharat B. Kale[a**] and Deepak R. Patil[a***]*

[a]Centre for Materials for Electronics Technology, Department of Electronics and Information Technology (DeitY), Govt. of India. Pune

[b]School of chemical sciences, Solapur university, Solapur, India

[c] Catalan Institute of Nanoscience and Nanotechnology (ICN2), and The Barcelona Institute of Science and Technology (CSIC-BIST), Campus UAB, Bellaterra, 08193 Barcelona, Spain

† Corresponding author. E-mail address: deepphy24@gmail.com (Dr. Deepak R. Patil), bbkale1@gmail.com (Dr. B. B. Kale), pedro.gomez@cin2.es (Prof. P. Gomez-Romero) Tel.: +91(020) 25898724; Fax: +91(020)25898085.

†These authors contributed equally

Abstract

The preparation of nanostructured hierarchical $Mn_xNi_{1-x}Co_2O_4$ metal oxides as efficient supercapacitors of different structures and configurations especially for the miniaturized electronics is still a challenge. In this context, we report template free facile hydrothermal synthesis of hierarchical nanostructured $Mn_xNi_{1-x}Co_2O_4$ with excellent supercapacitive performance. Significantly, the morphology of pure $MnCo_2O_4$ transformed from 3D microcubes to 1D nanowires with incorporation of Ni. The electrochemical study shows highest specific capacity i.e. 734 C/g for $Mn_{0.4}Ni_{0.6}Co_2O_4$ with high cycling stability of 89.2 % which is much higher than pristine $MnCo_2O_4$ and $NiCo_2O_4$. Later, asymmetric capacitor has been fabricated successfully using $Mn_{0.4}Ni_{0.6}Co_2O_4$ nanowires as positive electrode and activated carbon (AC) as negative electrode in a KOH aqueous electrolyte. An asymmetric cell could be cycled reversibly in the high-voltage range of 0 to 1.5 V and displays intriguing performances with a specific capacitance of 112.8 F/g (6.87 F/cm^3) and high energy density of 35.2 Wh/kg (2.1 mWh/cm^3). Importantly, this asymmetric capacitor device exhibits an excellent long cycle life along with 83.2 % specific capacitance retained after 2000 cycles.

Introduction

The fast-growing demand for eco-friendly, high power-density materials and devices have triggered significant research efforts. Generally, batteries are widely used for high energy-density applications like hybrid electric vehicles, power backup systems and computer backup. However, they have the limitations of high fabrication cost, low power density, limited cycle life etc. These limitations can be overcome by using supercapacitors which are ideal complementary storage devices since they have remarkable advantages such as high power density, long cycle life, fast charge/discharge capability, light weight, excellent reliability and flexibility [1]. However, in comparison to batteries they have low energy density. Hence, many efforts are being made to discover new materials and fabricate new supercapacitors with all the above mentioned advantages plus increased energy densities [2].

So far most of the research work is focused on redox-based electrode materials, including transition metal oxides and conducting polymers, because they exhibit much higher specific capacitances than carbon-based materials [3]. Among them, hydrous RuO_2 has been extensively studied as a typical supercapacitor material due to its high specific capacitance (1580 F/g) and excellent reversibility with high reliability [4]. However, its toxicity and high cost, prevent the realization of low-cost, high-performance electrode materials with more environmentally friendly and cost-effective properties.

In recent years, transition metal oxides such as MnO_2 [5], NiO [6], Co_3O_4 [7], $MnCo_2O_4$ [8] and $NiCo_2O_4$ [9] have been effectively employed as electrode materials for advanced supercapacitors, mostly because of their high specific capacitance, low cost, controllable structure, and unique morphology [9]. Among them, mixed transition metal oxides (MTMOs), especially ternary metal oxides with two different metal ions, have received an upsurge interest

as a promising supercapacitive electrode material [10]. A specially fruitful family of MTMOs exhibit a spinel structure corresponding to the formula AB_2O_4, in which A and B represent two different transition metals including Fe, Ni, Co, Mn, Zn, etc. In particular, the nickel cobaltite ($NiCo_2O_4$) and manganese cobaltite ($MnCo_2O_4$) spinels have been investigated not only for supercapacitor applications [8, 9] but also for water electrolysis (oxygen evolution) [11] and lithium-ion batteries [12]. Important properties of the spinel structures depend crucially on the exact nature of the cation distribution over the octahedral and tetrahedral sites in the spinel cubic lattice. Chemical substitution can tune the properties of these materials by altering this cation distribution. This influences the magneto-elastic properties of these materials, which can be explained in terms of the change in important physical/chemical properties. Moreover, the coupling of multiple metal species could render the MTMOs with rich redox reactions and improved electronic conductivity, which are beneficial to electrochemical applications. Among the various MTMOs, $MnCo_2O_4$ is one of the most promising candidates which has multiple valence states and is used as an anode for Li-ion batteries and drug delivery applications [13]. Despite its high potential for various applications in diverse fields, the electrical conductivity of $MnCo_2O_4$ is too low, [14] which limit its application in supercapacitors. On the other hand, $NiCo_2O_4$ possesses much better electronic conductivity and higher electrochemical activity than other MTMOs [15]. Therefore, by simply tuning the chemical compositions through substitution of Mn by Ni in $MnCo_2O_4$, one could greatly enhance the electronic conductivity as well as electrochemical activity. In this context, mixed manganese cobalt oxides ($MnCo_2O_4$) with various compositions of Mn and Ni will have great potential for electrochemical energy storage.

Another factor which strongly influences the performance of supercapacitors is the morphology of electrode materials. In particular, hierarchical nanostructures, such as assembly of

nanoparticles, nanorods, nanoplates, and nanosheets will undoubtedly provide a promising solution to enhance the performance of the supercapacitors because of their high surface areas, and short electron- and ion-transport pathways [16], while the microstructures, typically in micrometer or sub- micrometer dimension, would bring additional benefits, such as improved stability, uniform porosity, and resistance to aggregation. Therefore, the synthesis of MTMOs with controlled chemical composition as well as morphology is a challenging task, which has been demonstrated in the present work.

In the present investigation, we report the facile hydrothermal synthesis of nickel doped manganese cobalt oxide ($Mn_{1-x}Ni_xCo_2O_4$) hierarchical nanostructures with remarkable electrochemical supercapacitive performance. The electrochemical capacitances are investigated by cyclic voltammetry, galvanostatic charge/discharge and electrochemical impedance spectroscopy. Among the compositions, $Mn_{0.4}Ni_{0.6}Co_2O_4$ exhibits high specific capacity and excellent electrochemical activities. Later, an asymmetric capacitor AC/KOH/ $Mn_{0.4}Ni_{0.6}Co_2O_4$ nanowires was successfully assembled and studied. This supercapacitor presents an energy density of 35.2 Wh/kg, and also a rather good cycling performance.

Experimental

Synthesis of $Mn_{1-x}Ni_xCo_2O_4$ hierarchical structures:

All the reagents used were of analytical grade and used without further purification. In a typical synthesis, nickel substituted manganese cobaltate, $Mn_{1-x}Ni_xCo_2O_4$ (where x = 0.0, 0.2, 0.4, 0.6, 0.8 and 1.0) were successfully synthesized by hydrothermal method followed by calcinations. In this method each sample was prepared by taking the desired proportion of precursor acetates i.e. nickel acetate, manganese acetate and cobalt acetate and dissolved

separately in distilled water according to the stoichiometry. For example $Mn_{0.8}Ni_{0.2}Co_2O_4$ sample was prepared by taking 0.8 mM of manganese acetate, 0.2 mM of nickel acetate and 2 mM of cobalt acetate. After mixing the solutions, urea (4 mM) was added to this mixture. The mixture was then stirred until a homogeneous mixture was formed. This solution was then sealed into an autoclave for hydrothermal synthesis. The hydrothermal synthesis was carried out at 180˚C for 6 hrs. After being cooled to room temperature naturally, the precipitate was collected and washed with deionized water and ethanol for several times, dried at 60^{o}C for 4 h and then thermally treated at 400 °C for 3 h to obtain nanocrystalline $Mn_{0.8}Ni_{0.2}Co_2O_4$ powders. The $Mn_{1-x}Ni_xCo_2O_4$ samples with x = 0.0, 0.2, 0.4, 0.6, 0.8 and 1.0 were labelled as MCo, NMCo1, NMCo2, NMCo3, NMCo4, NCo, respectively.

Materials characterizations

The phase analysis of the samples were performed by X-ray diffraction (XRD) on a Rigaku-Ultima III with CuKα radiation (λ = 1.5418 Å). The surface morphology of as-prepared samples were investigated using the field-emission scanning electron microscopy (FEI Quanta 650F Environmental SEM) attached with an energy-dispersive X-ray spectroscopy (EDS) analyzer to measure the sample composition and transmission electron microscopy (Tecnai G2 F20 S-TWIN HR(S) TEM, FEI).The X-ray photoelectron spectra (XPS) analyses were obtained by X-ray photoelectron spectroscopy (XPS, SPECS Germany, PHOIBOS 150). The specific surface area was determined by the Brunauer-Emmett-Teller (BET) method. The working electrodes were prepared by using Doctor Blade technique. The paste of the $Mn_{1-x}Ni_xCo_2O_4$was prepared by mixing 85 % of active material with 10 % PVDF as binder and 5 % acetylene black. The prepared paste was then coated on the carbon cloth by using doctor blade method. The

resultant thin films were then annealed at 180^{o}C for two hours in order to remove the binder. The typical mass loading was found to be 0.56, 0.62, 0.41, 0.86, 0.91 and 0.8 mg/cm^2 for MCo, NMCo1, NMCo2, NMCo3, NMCo4 and NCo samples, respectively. The electrochemical properties were measured using standards three electrode system which contain working electrode ($Mn_{1-x}Ni_xCo_2O_4$), counter electrode (platinum) and reference electrode (Ag/AgCl) in 2 M KOH electrolyte. The all electrochemical measurements were carried out with Biologic VMP3 potentiostat. Asymmetric capacitor devices were assembled with $Mn_{0.4}Ni_{0.6}Co_2O_4$ (NMCo3) as the positive electrode (cathode) and activated carbon (AC) as the negative electrode (anode). The mass of active material in both electrodes was 4.2 mg. The electrodes were separated by polypropylene film separator soaked with 2 M KOH electrolyte.

Results and discussion:

Fig. 1 shows comparative XRD patterns of $Mn_{1-x}Ni_xCo_2O_4$ samples with x = 0.0, 0.2, 0.4, 0.6, 0.8 and 1.0. All of the diffraction peaks can be indexed to be cubic $MnCo_2O_4$ spinel structure (see supporting information S.I. S1 for standard reference). There is no impurity peaks observed, which indicates the high purity of the manganese nickel cobaltite. The broad reflection peaks are attributed to the nanocrystalline phase of $Mn_{1-x}Ni_xCo_2O_4$ samples. The XRD patterns of all the samples with different Mn:Co compositions are similar to the standard patterns of $MnCo_2O_4$ (JCPDS card no. 23-1237) indicating that the mixed manganese cobalt oxide also adopts the spinel structure with similar lattice constants. The XRD patterns of as-prepared materials (S.I. S2) correspond with nickel and cobalt carbonate hydroxide hydrate, which acts as precursor for synthesis of spinel $Mn_{1-x}Ni_xCo_2O_4$ material.

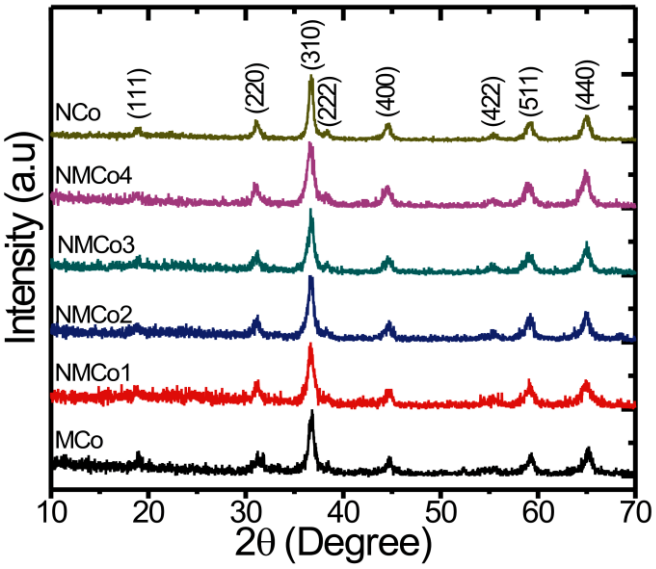

Fig. 1 XRD patterns of as-prepared MCo, NMCo1, NMCo2, NMCo3, NMCo4 and NCo samples calcined at 400 ^{0}C for 3 hrs.

In order to determine the element composition and oxidation state of the $Mn_{1-x}Ni_xCo_2O_4$ samples, X-ray photoelectron spectroscopy was subsequently conducted for NMCo3 sample (for full spectrum see S.I. S3) and de-convoluted spectra were illustrated in Fig. 2. Ni2p XPS spectra exhibit two major peaks with binding energy of 853.1 and 872.2 eV, respectively corresponding to the $Ni2p_{3/2}$ and $Ni2p_{1/2}$ energy levels, which is the signature characteristic of Ni^{2+} and Ni^{3+}. Moreover, two shakeup satellite peaks were observed at 861.1 and 879.2 eV, respectively [17]. The Mn 2p spectra seem to have two peaks at 642.2 and 653.7 eV (Fig. 2b), and they can be assigned to the Mn $2p_{3/2}$ and Mn $2p_{1/2}$ spin-orbit peaks. Fig. 2 (c) shows de-convoluted Co2p spectra, in which two major peaks with binding energy of 779.7 and 795.1 eV, respectively corresponding to the $Co2p_{3/2}$ and $Co2p_{1/2}$ energy level are observed. The high-resolution spectrum for the O1s region (Fig. 2d) shows three oxygen contributions, mainly at 529.6, 530.5 eV, and 531.6 eV, respectively. The O1s component located at 529.6 eV is typical of metal-

oxygen bonds. While the peak at 530.5 eV is usually associated with oxygen in OH^- groups and the presence of this contribution in the O1s spectrum indicates that the surface of the NMCo3 sample is hydroxylated to some extent as a result of either surface oxyhydroxide or the substitution of oxygen atoms at the surface by hydroxyl groups [18]. The peak at 531.6 eV corresponds to a higher number of defect sites with low oxygen coordination in the material with small particle sizes. These results show that the $NMCO_3$ sample exhibits a composition of Co^{2+}, Co^{3+}, Ni^{2+}, and Ni^{3+}, Mn^{2+}, and Mn^{3+}.

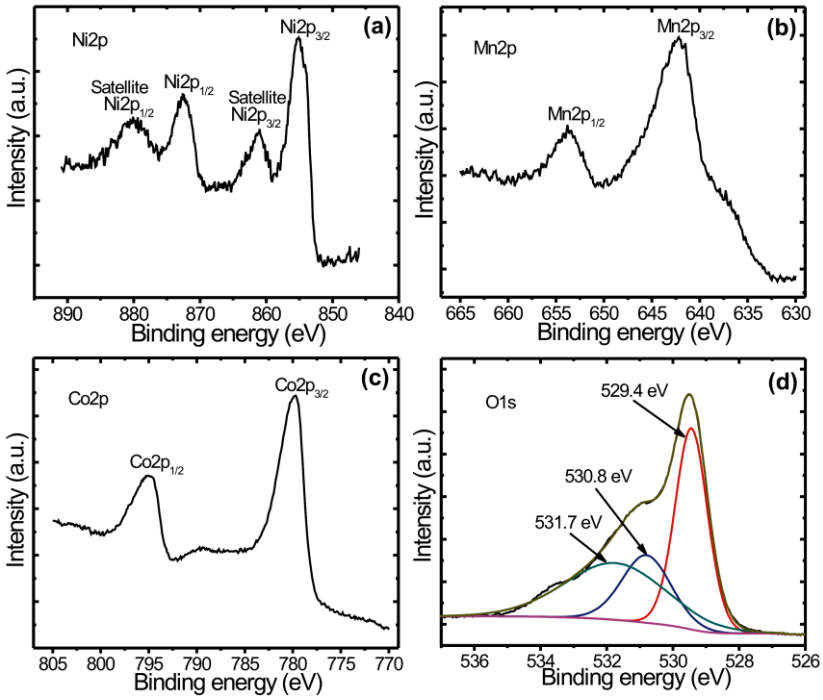

Fig. 2 (a) Ni 2p XPS spectrum (b) Mn 2p XPS spectrum (c) Co 2p XPS spectrum, and (d) O 1s XPS spectrum for the as-prepared NMCo3 nanowires.

A green and facile technique such as hydrothermal/solvothermal are well established to engineer nanostructures with unique and controlled morphologies. The morphologies obtained in these technique can be influenced by several factors like reaction promoters, reaction conditions

(mainly temperature and time), and synthesis methodology employed [19]. Fig. 3 shows the microstructure of $Mn_{1-x}Ni_xCo_2O_4$ materials synthesized under the same hydrothermal conditions. The observed morphologies are surprisingly transformed with the substitution of Ni-precursor in the reaction mixture (S.I. S4). The pristine $MnCo_2O_4$ exhibits cubic microstructure with interconnected morphology, as shown in Fig. 3 (a). Substitution of Ni in $MnCo_2O_4$ spinel, however, causes the material to grow in the form of nanowires, as shown in Fig. 3 (b-f), which can have higher surface area and uniform porosity compared to the cubic morphology of $MnCo_2O_4$. Initial substitution of Ni ($Mn_{0.8}Ni_{0.2}Co_2O_4$) doesn't have considerable effect on the morphology, maintaining the cubic microstructure. However, further substitution of Ni resulted in the dissolution of cube and transformation to nanowires (Fig 3c). It is clear that the nanowires have high aspect ratios with lengths of up to several micrometers and diameters down to several nanometers. This sudden change in the microstructure is mainly ascribed to Ni insertion into $MnCo_2O_4$ spinel lattice during the synthesis. It is interesting to note that the length of the nanowires obtained was further reduced at higher concentration of Ni. It is well-known that crystallographic shapes are composed of crystallographic planes, which are further related to the surface energies. In addition, it is also established that adsorption of organic and inorganic additives on certain crystallographic planes can alter the relative order of surface energies during the crystal growth process [20]. This preferential adsorption lowers the surface energy and directs the formation of a particular morphology of the material. In the present case, incorporation of Ni on the crystallographic plane of $MnCo_2O_4$ might have modified the surface energies for the formation of cubic structure and transformed the respective surface energies for the growth of nanowires. The pristine structure of Mn is body centered and Ni is face centered cubic. The face centered cubic structure of Ni has tendency of one dimensional growth as

compare to Mn i.e. body centered cubic structure. Therefore, incorporation of Ni into Mn accelerates one dimensional growth under hydrothermal condition. Hence, the morphology of pristine $MnCo_2O_4$ was changed to nanowires after the substitution of Ni precursor in hydrothermal reaction mixture. These nanowires of $Mn_{1-x}Ni_xCo_2O_4$ make it a unique material and superior as an electrode for supercapacitors.

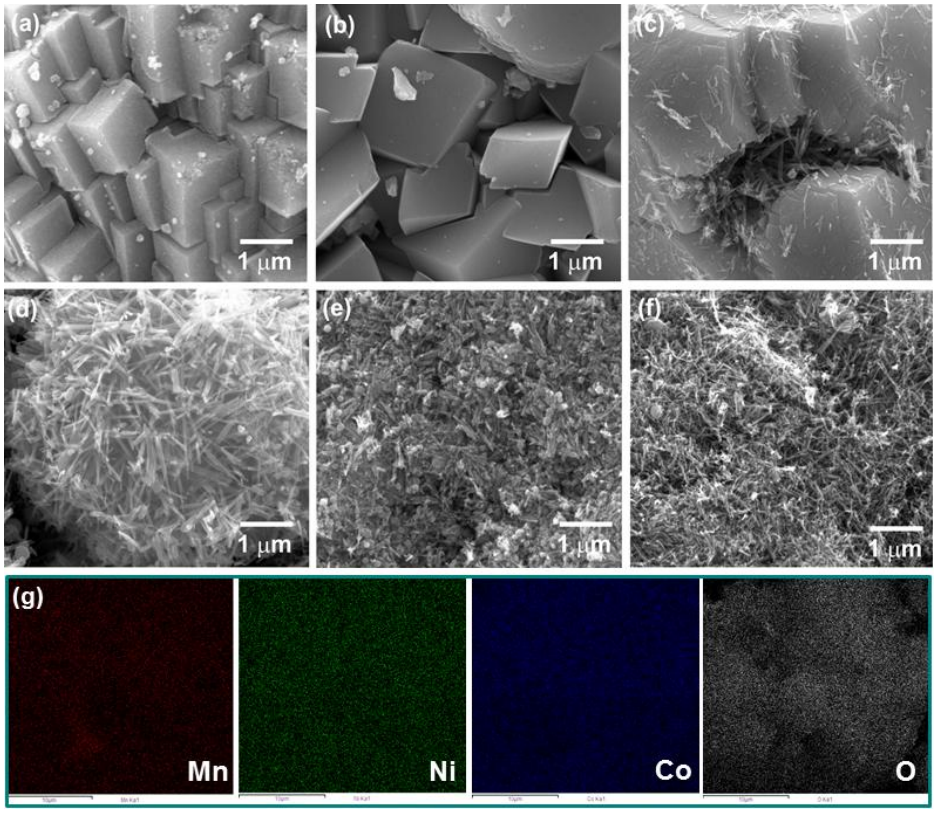

Fig. 3 FE-SEM images of as synthesized (a) MCo (b) NMCo1 (c) NMCo2 (d) NMCo3 (e) NMCo4 (f) NCo and (g) corresponding element mappings of NMCo3 sample.

This unique 1D nanowires-like $Mn_{1-x}Ni_xCo_2O_4$ can provide high accessible surface for electrolyte ions as well as short diffusion path for intercalation/de-intercalation which is beneficial to energy storage application. Furthermore, EDS mapping of a single NMCo3 nanorod is shown in Fig. 3 (g) unambiguously confirms the presence of Mn, Ni, Co and O elements on

the entire surface of the material. The elemental mapping of other samples is given in Fig. S. I. S5.

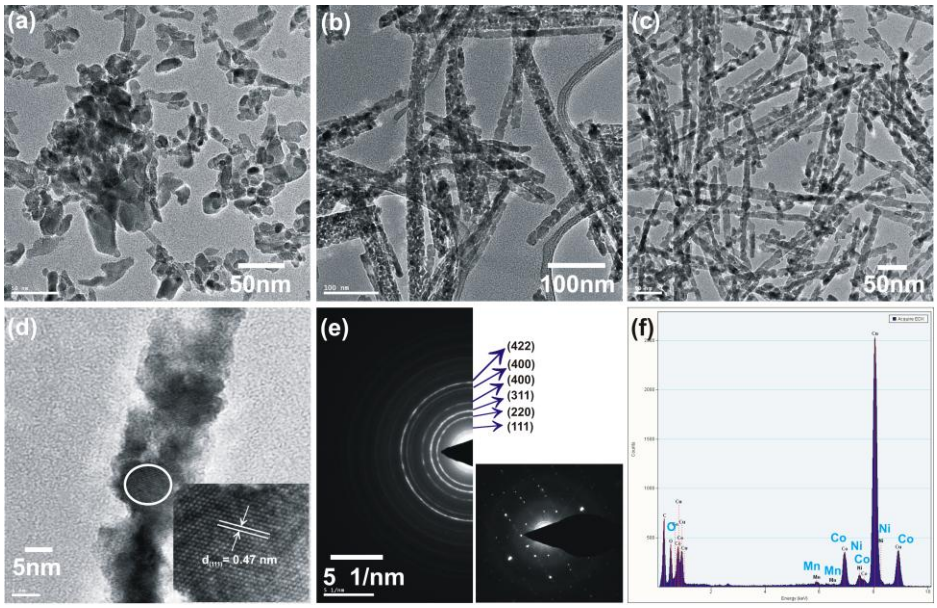

Fig. 4 TEM images of (a) MCO, (b) NMCo3nanowires and (c) NCO samples (d) HRTEM image of NMCo3 and Inset shows a higher magnification image of the NMCo3 nanowires (e) shows the corresponding SAED pattern NMCo3 nanowires and (f) shows elemental analysis of NMCo3 nanowires

The microstructure and morphology of the $Mn_{1-x}Ni_xCo_2O_4$ nanorods was also investigated by using transmission electron microscopy (TEM). Fig. 4 (a-c) shows TEM images of MCo, NMCo3 and NCo samples, respectively. As illustrated in Fig. 4 (a), MCo sample exhibits distorted small parts of cubes. This clearly confirms the formation of interconnected micro-structured cubes through the collection of small nanocubes. Further, the $Mn_{1-x}Ni_xCo_2O_4$ nanowires (Fig. 4 b, c) have a porous structure with diameter of about 10 nm and the nanowires are composed of tiny nanocrystallites of size few nanometers, which agree well with the FE-

SEM results. The high resolution TEM image of single nanowire suggests that the nanowires are composed of nanoparticles aligned in one dimension with diameters ranging from 5-15 nm (Fig. 4 (d)). One dimensional nanowire may contribute to the higher capacitance because of the increased electrochemical active sites and short ion transport pathway [21]. The inset of Fig. 4 (d) demonstrates the HRTEM image of a single porous nanowire of NMCo3 sample. The lattice fringes show the structural characteristic of the cubic spinel $MnCo_2O_4$ crystal, in which the d-spacing of 0.47 marked in the pattern could be indexed to the (111) plane of cubic spinal structure, which further confirmed the formation of crystalline NMCo3 nanowires and agreed well with the XRD data. The SAED pattern, which has been detected from a sampling area covering a collection of several nanowires, shows well-defined rings (Fig. 4e), indicating the unique nanolycrystalline nature of NMCo3. The EDX spectrum of the nanowires is presented in Fig. 4 (f), which further reveals the presence of Ni, Mn, Co, and O elements. The EDX spectra of other samples have been given in the Fig. S. I. S6. The unique morphologies observed for the present samples are likely to make promising materials for supercapacitor applications.

The BET specific surface area of MCo, NMCo3 and NCo samples were determined by N2 adsorption/desorption measurement (one point BET surface area). The NMCo3 ($Mn_{0.4}Ni_{0.6}Co_2O_4$) hierarchical nanostructure exhibits relatively high BET surface area of 60.58 m^2/g than that of samples MCo (32.51 m^2/g) and NCO (37.12 m^2/g), respectively. This is probably due to the open pores formed by the nanoparticles in the NMCo3 nanowires (also evident from the TEM results), resulted in a high one point surface area. The BET results indicate that the substitution of Ni into $MnCo_2O_4$ greatly enhances the surface area and therefore improves the capacitive performance of the composite electrode effectively.

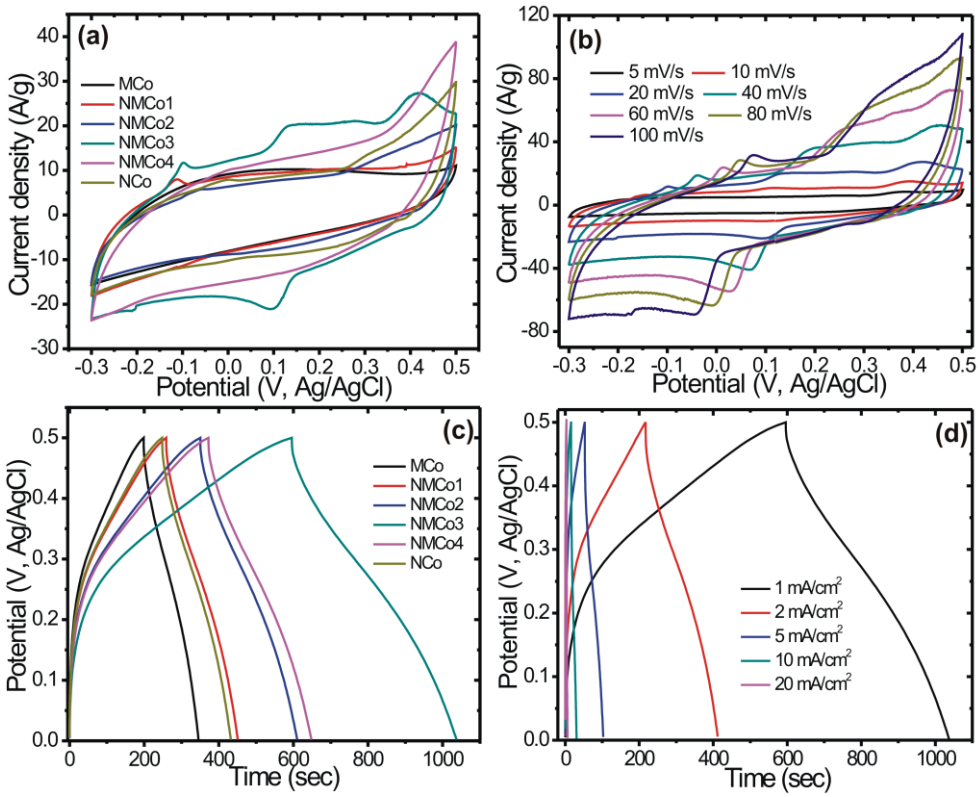

Fig. 5 (a) Cyclic voltammetry (CV) curves of MCo, NMCo1, NMCo2, NMCo3, NMCo4 and NCO within 0.5 V at a scan rate from 40 mV/s in 2 M KOH electrolyte. (b) CV measurements of NMCo3 sample at different scan rate from 5 to 100 mV/s (c) Galvanostatic charge-discharge curves of MCo, NMCo1, NMco2, NMco3, NMCo4 and NCO samples at current density of 1 mA/cm^2, (d) Galvanostatic charge/discharge curves of NMCo3 sample at different current densities.

This unique hierarchical nanostructure encourages us to further investigate electrochemical performances of $Mn_{1-x}Ni_xCo_2O_4$ samples. Fig. 5 (a) shows the cyclic voltammetry (CV) curves of the $Mn_{1-x}Ni_xCo_2O_4$ single electrodes (3-electrode configuration) at a fixed scan rate of 5 mV/s. It can be observed that the CV curves of all the samples consists of pairs of broad and poorly defined redox peaks, which are associated with the redox reactions. It

is interesting to note that, with increase in concentration of Ni-substitution, the current under the curve increases until x=0.6 (NMCo3 sample) and then begins to decrease. Impressively, the intensity of redox peaks for NMCo3 ($Mn_{0.4}Ni_{0.6}Co_2O_4$) sample is relatively higher than other samples suggesting excellent interaction of NMCo3 nanowires with electrolyte. In addition, slim and elongated nanowires allow fast diffusion and large electrochemical active sites. Fig. 5 (b) show the CV curves of the NMCo3 sample at different scan rates. As scan rate increases, the shape of the CV curves remains unchanged, thus indicating the excellent electrochemical reversibility and outstanding high-rate performance. However, the redox peaks shifted towards lower potential, which may due to the polarization effect of the electrodes. Further, Fig. 5 (c) shows the galvanostatic charge/discharge measurements of all the samples at current density of 1 mA/cm^2. These curves are symmetric, indicating a good electrochemical characteristic and superior reversible redox reaction. It is worth noting that, the NMCo3 sample exhibits high discharge time compared to other samples. Fig. 5 (d) shows charge/discharge curves for NMCo3 sample at different current densities. The CD curves are still symmetrical even at high current densities, an indication of high rate capacity.

The variation of specific capacity with current density for the $Mn_{1-x}Ni_xCo_2O_4$ samples is shown in Fig. 6 (a). The higher specific capacity is observed at lower current density of 1 mA/cm^2, for all the samples and it steadily decreases with the increasing current density. This is mainly due to the fact that the high current density prevents the accessibility of ions from entering into all the inner microstructures of the electrode material, and thus the transport of ions is limited (due to their slow diffusion) and only the outer surface can be utilized for charge storage [22]. Thus, the Ni substituted $MnCo_2O_4$ hierarchical structures exhibit high specific capacity and excellent rate capability as compared to pristine NCo and MCo samples. The

maximum specific capacity of 734 C/g is observed for NMCo3 sample. The long-term cycling stability is another crucial parameter to confirm the practical applicability electrodes; therefore the cycling stability of NCo, MCo and NMCo3 samples were executed at 9 A/g using charge/discharge test over 3000 cycles. The plot of specific capacity retention versus number of cycles is shown in Fig. 6 (b). It is observed that the NMCo3 sample demonstrates relatively high capacity retention of 89.2 % over 2000 charge/discharge cycles suggesting good cycling stability which is highly desirable in high performance energy storage devices. Further, the electrochemical impedance analysis was carried out to investigate the electrical conductivity of $Mn_{1-x}Ni_xCo_2O_4$ samples and is presented in Fig. 6 (c). All the $Mn_{1-x}Ni_xCo_2O_4$ electrodes exhibit almost same equivalent series resistance (ESR) 0.12-0.23 Ω cm^2 while NMCo3 sample provides relatively low charge transfer resistance 5.1 Ω cm^2. Low ESR and charge transfer resistance for NMCo3 sample ($Mn_{0.4}Ni_{0.6}Co_2O_4$) reveals relatively high conductivity.

These exceptional electrochemical properties of NMCo3 sample are mainly attributed to the synergetic effect of morphology and chemical compositions such as: i) the growth of nanowires offers high active surface area for facile electron transport, leading to faster kinetics and higher utilization of active material, ii) the substitution of Ni into Mn sites can alter the cation distribution over tetrahedral and octahedral sites thereby tuning its electrochemical properties. The substitution of Ni into Mn goes into the octahedral sites which introduces electrochemical redox reaction to boost the charge storage capability.

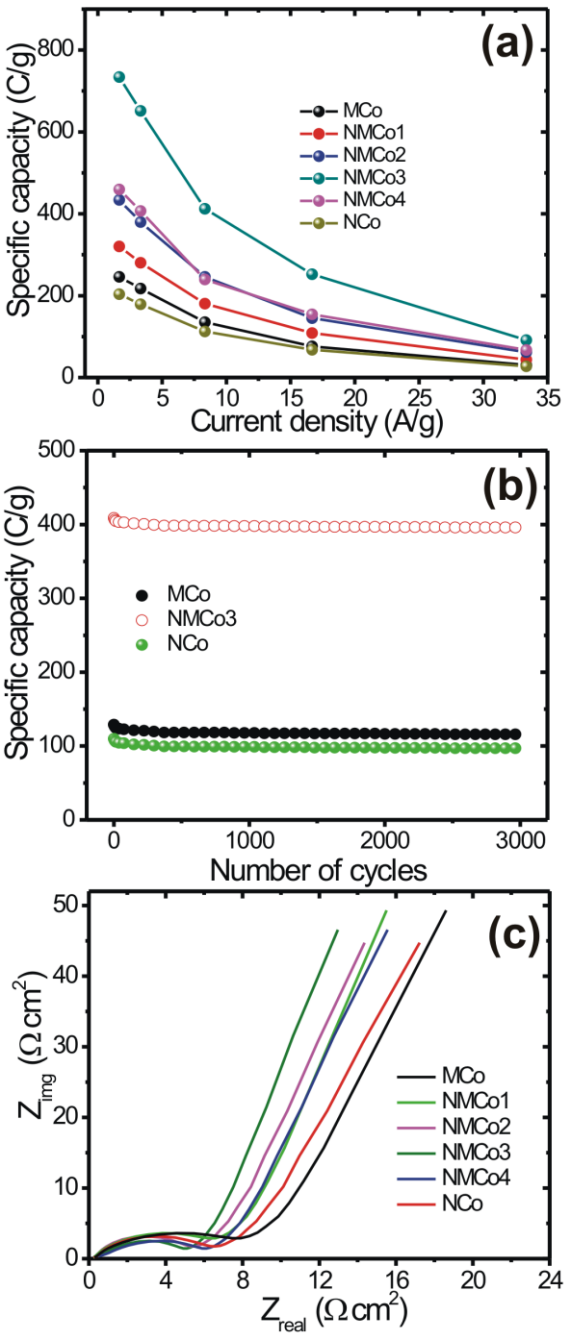

Fig. 6 (a) Variation of specific capacity (C/g) of MCo, NMCo1, NMco2, NMco3, NMCo4 and NCO samples with current density, (b) Variation of specific capacity with cycle number for MCo, NMCo3 and NCo samples over 3000 cycles (c) Nyquist plots for MCo, NMCo1, NMco2, NMco3, NMCo4 and NCO samples with amplitude 5 mV in 1 mHz to 10 kHz

Asymmetric capacitors using NMCo3 ($Mn_{0.4}Ni_{0.6}Co_2O_4$) as the positive electrode and activated carbon (AC) as the negative electrode

Considering the excellent electrochemical properties of NMCo3 ($Mn_{0.4}Ni_{0.6}Co_2O_4$) electrode and the fast ion-transport property of activated carbon (AC) material, an asymmetric capacitor was successfully fabricated using these materials as the positive and negative electrodes, respectively. Fig. 7 (a) show the CV curves for AC and NMCo3 single electrodes at a scan rate of 10 mV/s. As seen in Fig. 7 (a), the CV curve of AC electrode showed an ideal rectangular shape without hydrogen evolution at -1.0 V (Ag/AgCl), which was the characteristic of the electric double layer capacitance. Moreover, CV curve with well-defined redox peaks for NMCo3 sample is shown in -0.3 to +0.5 V (Ag/AgCl). This suggests that, these two materials are greatly stable in different potential windows. Consequently, if the total cell voltage can be expressed as the sum of the potential range for NMCo3 electrode and AC, it is possible to conclude that the cell potential can be extended up to 1.5 V in for an asymmetric capacitor. The specific electric quantity of AC at 1 mA/cm^2 charge/discharge current was 262.6 C/g. While the NMCo3 electrode exhibits a high specific capacity 743 C/g. The specific capacity ratio found for the AC and NMCo3 was 1:0.44. This is due to the different charge-storage mechanisms between the two materials. It should be noted that, to approach the highest cell voltage, the charges stored in both electrodes must be balanced by adjusting the mass loading of each of the active electrode materials [23]. The AC to NMCo3 mass ratio was calculated by the following equation:

$$\frac{m_+}{m_-} = \frac{q_-}{q_+} \qquad (1)$$

On the basis of the specific capacity values found for NMCo3 and AC, the optimal mass ratio between the electrodes should be m(AC)/m(NMCo3) = 1:0.44 in the asymmetric capacitor

cell. Generally, the capacity of the negative electrode is higher than that of the positive electrode in an asymmetric capacitor. In present investigation, the mass loadings of NMCo3 and AC electrodes were adjusted to 1.2 mg/cm^2 and 2.7 mg/cm^2 in the asymmetric cell (3.9 mg total mass of active materials in both electrodes). An asymmetric capacitor, AC//NMCo3, was assembled by using aqueous 2 M KOH electrolyte. Fig. 7 (b) show the CV curves of the AC//NMCo3 asymmetric cell measured at various scan rates from 5-200 mV/s between 0 and 1.5 V. As seen, the CV curve of this cell exhibited a large current area with broad redox peak, which is the characteristic of the electric double layer capacitance and Faradaic pseudo-capacitance. The shape of the CV remains unchanged even at a high scan rate of 200 mV/s, suggesting excellent rate capability. Further, galvanostatic charge/discharge curves of the asymmetric cell were recorded with various current densities and are presented in Fig. 7 (c). A nonlinear relation of the charge/discharge potentials with time was found. In addition, the initial voltage loss (i.e., iR drop) observed in the discharge curves is small even at high current densities; this is indicative of fast I-V response and low internal resistance of the supercapacitors. Additionally, from the typical galvanostatic CD curves, it can be observed that the discharge curve is nearly symmetric with its corresponding charging counterpart, demonstrating the excellent electrochemical reversibility and good coulombic efficiency. The specific capacitance during the galvanostatic charge/discharge process is calculated using following equation:

$$C = \frac{2 \cdot I \cdot \int V \cdot dt}{m \cdot V^2} \qquad (2)$$

where, I is the discharge current, Δt is the discharge time, m is the mass of the active material (both electrodes, 3.9 mg) and ΔV is the potential window. The calculated specific and volumetric capacitance for AC//NCMo3 asymmetric cell at different current densities is shown

in Fig. 7 (d). The maximum capacitance obtained for cell is 112.8 F/g (6.87 F/cm^3, considering volume of device 0.0689 cm^3) at current density of 1.2 A/g. A higher specific capacitance could be obtained in a higher operation voltage window thanks to the redox reactions of NMCo3 electrode.

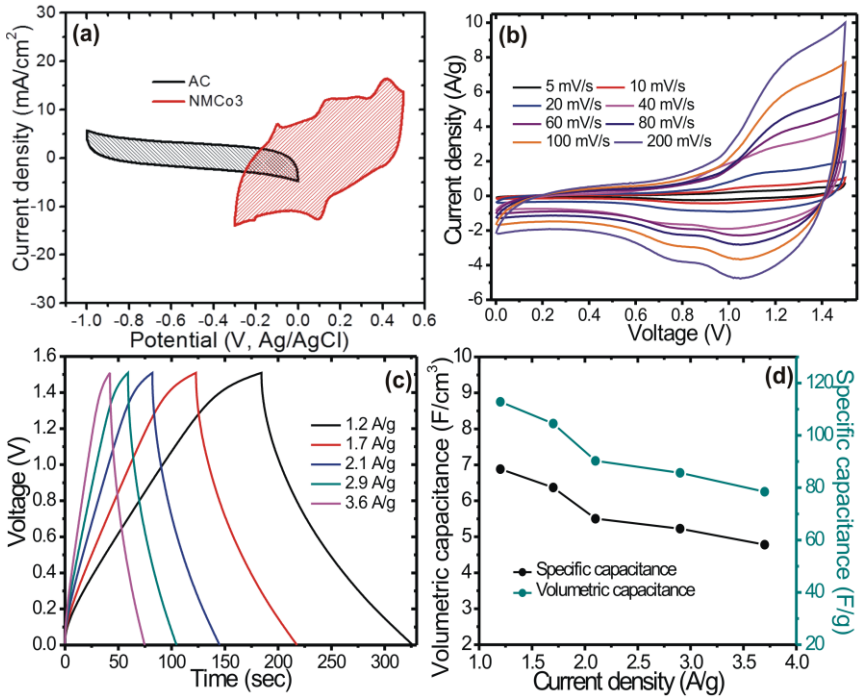

Fig. 7 (a) CV curves of activated carbon (AC) and NMCo3 samples within different operating potential windows at constant scan rate of 10 mV/s (b) CV curves of AC//NMCo3 asymmetric cell within operating voltage window of 1.5 V at various scan rates (c) Galvanostatic charge/discharge curves of AC//NMCo3 asymmetric cell at different current densities (d) Plots of volumetric and specific capacitances with current density for AC//NMCo3 asymmetric cell

Since it is vital to retain high specific capacitances (or energy density) at high current density, we estimated the energy and power density, which are key factors for the supercapacitor applications by using following equation:

$$E = \frac{1}{2} C \Delta V^2 \quad (3)$$

$$P = \frac{E}{\Delta t} \times 3600 \quad (4)$$

where, E is the specific energy density, C refers to the specific or volumetric capacitance, ΔV is the voltage range, P represents the power density, and Δt is the discharge time. The Ragone plots are presented in the Fig. 8 (a, b). The energy density of the AC//NMCo3 asymmetric cell based on the total mass of the active electrode materials (including AC and NMCo3) reaches 35.3 Wh/kg (2.1 mWh/cm^3) at a power density of 892 W/kg (54 mW/cm^3), and still remains 24. 5 Wh/kg (1.4 mWh/cm^3) at a power density of 2678 W/kg (163 mW/cm^3). Interestingly, the maximum energy density obtained for AC//NMCo3 asymmetric capacitor with a cell voltage of 1.5 V is much higher than those of symmetric AC/AC supercapacitor (<10 Wh/kg) [24], graphene/graphene (9.1Wh/kg) [25], CNT/CNT supercapacitor (<10 Wh/kg) [26], and asymmetric supercapacitors with aqueous electrolyte solutions, such as Ni-Co oxy-hydroxide//AC (17.8 Wh/kg) [27], $NiCo_2O_4$-RGO//AC (12 and 23.3 Wh/kg) [27, 28], $NiCo_2O_4$//AC (15.32 and 17.72 Wh/kg) [29, 30], $NiCo_2O_4$-graphene//AC (7.6 Wh/kg) [31], Ni-Co oxide//activated graphene (53 Wh/kg) and Ni-Co oxide//activated polyaniline derived carbon (71.7 Wh/kg) [32], RGO//$NiCo_2O_4$ (23.9 Wh/kg) [33], AC//$NiCo_2O_4$-AC (14.7 Wh/kg) [34], AC//$NiCo_2O_4$@MnO_2 (35 Wh/kg) [35]. Therefore, the considerably high energy density derived by this simple AC//NMCo3 asymmetric cell has important industrial applications in the field of supercapacitors. The cycling life test over 2000 cycles for the AC//NMCo3 asymmetric capacitor was carried out by repeating the charging/discharging test between 0 and 1.5 V at a current density of 3.7 A/g. Fig. 8 (c) shows the cycle performance of the asymmetric capacitor charged at 1.6 V as a function of the cycle number. The asymmetric cell exhibits excellent

electrochemical stability of 83.2 % over 2000 cycles. The results demonstrated AC//NMCo3 asymmetric cell displayed a high specific capacitance and excellent cycling stability.

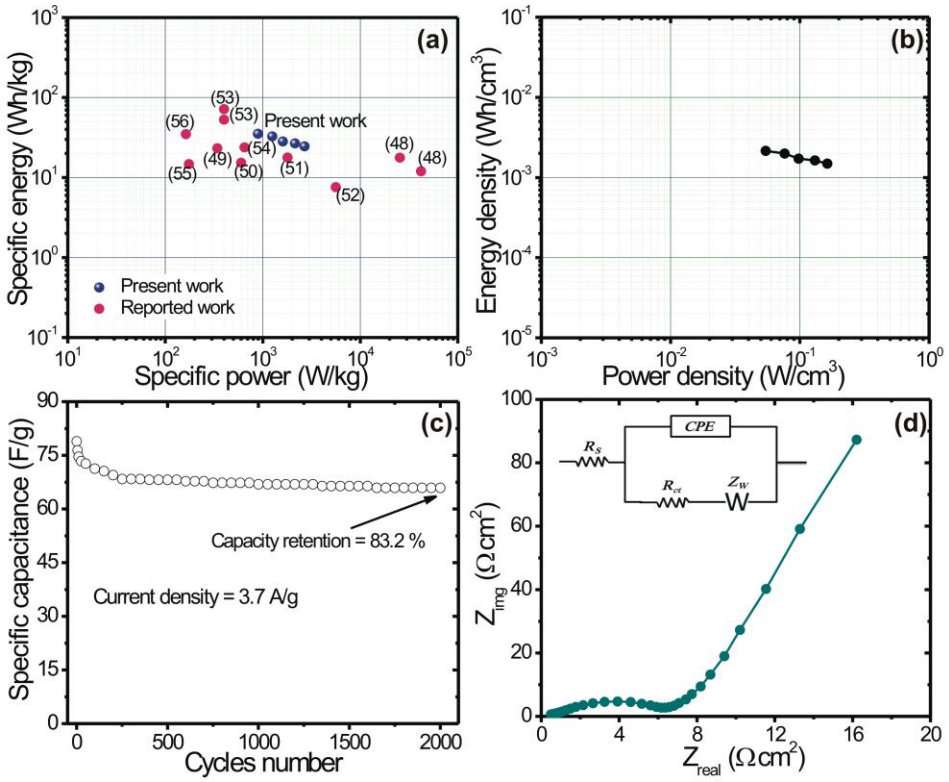

Fig. 8 (a, b) Plots of energy density versus power density of AC//NMCo3 asymmetric cell in Ragone plot, (c) Variation of specific capacitance with number of cycles measured at 3.7 A/g over 2000 cycles, (d) Nyquist plot of AC//NMCo3 cell within a frequency range of 1 KHz to 0.1 mHz

EIS of AC//NMCo3 asymmetric capacitor was measured at open circuit potential and the Nyquist plot is shown in Fig. 8 (d) with inset representing the equivalent circuit R_s, solution resistance; R_{ct}, charge transfer resistance; CPE denote constant-phase elements and Z_w is Warburg's impedance. Generally, the depressed semicircle in the high-frequency range represents the charge-transfer resistance (R_{ct}) caused by the Faradaic reactions and the double-

layer capacitance on the grain surface. The charge-transfer resistance for AC//NMCo3 asymmetric cell was found to be 6.2 Ω cm^2. The slope of the 45° portion of the curve is called the Warburg resistance and is a result of the frequency dependence of ion diffusion/transport in the electrolyte to the electrode surface.

Conclusions

In conclusion, we have synthesized $Mn_{1-x}Ni_xCo_2O_4$ hierarchical nanostructures by using a template free facile hydrothermal method. These hierarchical structures transformed from 3D micro cubes to 1D nanowires with increasing Ni:Mn substitution into $MnCo_2O_4$. The doped $Mn_{1-x}Ni_xCo_2O_4$ electrodes exhibit high electrochemical performance as compared to pristine $MnCo_2O_4$ and $NiCo_2O_4$ samples. Among the different ratios of nickel to manganese, $Mn_{0.4}Ni_{0.6}Co_2O_4$ (mixture of $NiCo_2O_4$ and $MnCo_2O_4$) offers excellent electrochemical properties. An asymmetric capacitor based on $Mn_{0.4}Ni_{0.6}Co_2O_4$ as positive electrode and AC as negative electrode (AC// $Mn_{0.4}Ni_{0.6}Co_2O_4$) exhibits a specific capacitance of 112.8 F/g (6.87 F/cm^3) and high energy density of 35.3 Wh/kg (2.1 mWh/cm^3). This work demonstrates that the direct use of these kinds of electrodes as positive electrode for asymmetric supercapacitor is feasible. Furthermore, the unique nano-architecture of this electrode may have potential applications in lithium ion batteries, water splitting, photodetector etc.

Acknowledgements

The authors would like to thank the Department of Science and Technology (DST, New Delhi) INSPIRE faculty program and the Department of Electronics and Information Technology (DeitY, New Delhi) for financial support for this work. The authors wish to thank Nanocrystalline Material and Glass laboratory, C-MET Pune for their generous help. DPD and PGR appreciate the award with the support of the Secretary for

Universities and Research of the Ministry of Economy and Knowledge of the Government of Catalonia and the Co-fund programme of the Marie Curie Actions of the 7th R&D Framework Programme of the European Union. ICN2 acknowledges support of the Spanish MINECO through the Severo Ochoa Centers of Excellence Program under Grant SEV-2013-0295. D. P. Dubal and P. Gomez-Romero acknowledge AGAUR (Generalitat de Catalunya) for Project NESTOR (Nanomaterials for Energy STORage) 2014_SGR_1505

References

[1] (a) D. P. Dubal, O. Ayyad, V. Ruiz, P. Gomez-Romero, *Chem. Soc. Rev.*, 2015, **44,** 1777, (b) G. Wang, L. Zhang J. Zhang, *Chem. Soc. Rev.*, 2012, **41**, 797, (b) K. Naoi, S. Ishimoto, J. Miyamoto, W. Naoi, *Energy Environ. Sci.*, 2012, **5**, 9363, (d) D. P. Dubal, J. G. Kim, Y. Kim, R. Holze, C. D. Lokhande, W. B. Kim, *Energy Technol.* 2014, **2**, 325.

[2] (a) J. R. Miller, P. Simon, *Science*, 2008, **321**, 651, (b) L. Cao, F. Xu, Y. Y. Liang, H. L. Li, *Adv. Mater.*, 2004, **16**, 1853, (c) P. H. Yang, X. Xiao, Y. Z. Li, Y. Ding, P. F. Qiang, X. H. Tan, W. J. Mai, Z. Y. Lin, W. Z. Wu, T.Q. Li, H. Y. Jin, P. Y. Liu, J. Zhou, C. P. Wong, Z. L. Wang, *ACS Nano*, 2013, **7**, 2617.

[3] (a) R. Liu, S. B. Lee, *J. Am. Chem. Soc.*, 2008, **130**, 2942, (b) T. Zhu, J. S. Chen, X. W. Lou, *J. Mater. Chem.*, 2010, **20**, 7015, (c) G. H. Zhang, Y. J. Chen, B. H. Qu, L. L. Hu, L. Mei, D. N. Lei, Q. Li, L. B. Chen, Q. H. Li, T. H. Wang, *Electrochim. Acta*, 2012, **80** 140

[4] (a) W. Wang, S. Guo, I. Lee, K. Ahmed, J. Zhong, Z. Favors, F. Zaera, M. Ozkan, C. S. Ozkan, *Sci. Rep.*, 2014, **4**, 4452 (b) S. C. Hong, S. Kim, W. J. Jang, T. H. Han, J. P. Hong, J. S. Oh, T. Hwang, Y. Lee, J. H. Lee, J. D. Nam, RSC Adv. 2014, **4**, 48276

[5] D. P. Dubal, J. G. Kim, Y. Kim, R. Holze, W. B. Kim, *Energy Technol.*, 2013, **1**, 125.

[6] C. Yuan, J. Li, L. Hou, L. Yang, L. Shen, X. Zhang, *Electrochim. Acta*, 2012, **78**, 532

[7] C. Yuan, L. Yang, L. Hou, L. Shen, X. Zhang, X. W. Lou, *Energy Environ. Sci.*, 2012, **5**, 7883

[8] (a) H. Jiang, J. Ma, C. Li, *Chem. Commun.*, 2012, **48**, 4465, (b) Y, Guo, L. Yu, C. Y. Wang, Z. Lin, X. W. Lou, *Adv. Funct. Mater.*, 2015, **25**, 5184, (c) Y. Xu, X. Wang, C.

An, Y. Wang, L. Jiao, H. Yuan, *J. Mater. Chem. A*, 2014, **2**, 16480, (d) A. K. Mondal, D. Su, S. Chen, A. Ung, H. S. Kim, G. Wang, *Chem. Eur. J.*, 2015, **21**, 1526

[9] (a) J. Jiang, Y. Li, J. Liu, X. Huang, C. Yuan and X. W. Lou, *Adv. Mater.*, 2012, **24**, 5166, (b) L. Yu, B. Guan, W. Xiao, X. W. Lou, *Adv. Energy Mater.*, 2015, **5**, 1500981, (c) Y. M. Chen, Z. Li, X. W. Lou, *Angew. Chem. Int. Ed.*, 2015, **54**, 10521

[10] D. P. Dubal, P. Gomez-Romero, B. R. Sankapal, R. Holze, *Nano Energy* 2015, **11**, 377.

[11] (a) B. Chi, J. B. Li, Y. S. Han, Y. J. Chen, *Int. J. Hydrogen Energy*, 2004, **29**, 605, (b) E. B. Castroa, S. G. Reala, L. F. Pinheiro Dick, *Int. J. Hydrogen Energy*, 2004, **29**, 255.

[12] (a) R. Alcántara, M. Jaraba, P. Lavela, J. L. Tirado, *Chem. Mater.*, 2002, **14**, 2847, (b) A. V. Chadwick, S. L. P. Savin, S. Fiddy, R. Alcantara, D. F. Lisbona, P. Lavela, G. F. Ortiz, J. L. Tirado, *J. Phys. Chem. C*, 2007, **111**, 4636.

[13] K. V. Sankar, R. K. Selvan, *RSC Adv.*, 2014, **4**, 17555

[14] (a) H. Jiao, *J. Mater. Eng. Perform.*, 2011, 20, 1638, (b) Y. Li, J. Jiang, J. Zhao, *Chem. Phys.*, 2004, 87, 91.

[15] (a) T. Y. Wei, C. H. Chen, H. C. Chen, S. Y. Lu, C. C. Hu, *Adv. Mater.*, 2010, **22**, 347, (b) H. L. Wang, Q. M. Gao, L. Jiang, *Small*, 2011, **7**, 2454, (c) G. Q. Zhang, H. B. Wu, H. E. Hoster, M. B. Chan-park, X. W. Lou, *Energy Environ. Sci.*, 2012, **5**, 9453, (d) C. Z. Yuan, J. Y. Li, L. R. Hou, X. G. Zhang, L. F. Shen, X. W. Lou, *Adv. Funct. Mater.*, 2012, **22**, 4592.

[16] (a) G. B. Sun, B. X. Dong, M. H. Cao, B. Q. Wei, C. W. Hu, *Chem. Mater.*, 2011, **23**, 1587, (b) B. Wang, J. S. Chen, H. B. Wu, Z. Y. Wang, X. W. Lou, *J. Am. Chem. Soc.*, 2011, **133**, 17146, (c) H. B. Wu, X. W. Lou, H. H. Hng, *Chem. Eur. J.*, 2012, **18**, 2094.

[17] (a) J. F. Marco, J. R. Gancedo, M. Gracia, J. L. Gautier, E. I. R´ıos, H. M. Palmer, C. Greavesc, F. J. Berry, *J. Mater. Chem.*, 2001, **11**, 3087, (b) Y. E. Roginskaya, O. Morozova, E. Lubnin, Y. E. Ulitina, G. Lopukhova, S. Trasatti, *Langmuir*, 1997, **13**, 4621.

[18] T. Choudhury, S. O. Saied, J. L. Sullivan, A. M. Abbot, *J. Phys. D: Appl. Phys.*, 1989, **22**, 1185.

[19] F. I. Pires, E. Joanni, R. Savu, M. A. Zaghete, E. Longo, J. A. Varela, *Mater. Lett.* 2008, **62**, 239

[20] M. J. Siegfried, K. S. Choi, *Adv. Mater.*, 2004, **16**, 1743

[21] H. Wu, Z. Lou, H. Yang, G. Shen, *Nanoscale*, 2015, **7**, 1921

[22] (a) G. Zhang, T. Wang, X. Yu, H. Zhang, H. Duann, B. Lun, *Nano Energy*, 2013, **2**, 586, (b) X. X. Xia, J. P. Tu, Y. Q. Zhang, X. L. Wang, C. D. Gu, X. B. Zhao, H. J. Fan, *ACS Nano*, 2012, **6**, 5531.

[23] (a) D. P. Dubal, R. Holze, P. Gomez-Romero, *Sci. Rep.*, 2014, **4**, 7349, (b) D. P. Dubal, N. R. Chodankar, G. S. Gund, R. Holze, C. D. Lokhande, P. Gomez-Romero, *Energy Technol.* 2015, **3**, 168-176

[24] (a) C. Zheng, L. Qi, M. Yoshio, H. Wang, J. Power Sources, 2010, **195**, 4406, (b) D. W. Wang, F. Li, M. Liu, G. Q. Lu, H. M. Cheng, Ang. Chem. Int. Ed., 2008, 47, 373, (c) V. Khomenko, E. Raymundo-Piñero, F. Béguin, J. Power Sources, 2010, **195,** 4234

[25] H. Wang, Y. Liang, T. Mirfakhrai, Z. Chen, H. Casalongue, H. Dai, *Nano Res.* 2011, **4**, 729

[26] (a) C. Yu, C. Masarapu, J. Rong, B. Wei, H. Jiang, *Adv. Mater.* 2009, **21**, 4793, (b) Y. Honda, T. Haramoto, M. Takeshige, H. Shiozaki, T. Kitamura, M. Ishikawa, *Electrochem. Solid-State Lett.*, 2007, **10**, A106

[27] C. C. Hu, C. T. Hsu, K. H. Chang, H. Y. Hsu, *J. Power Sources*, 2013, **238**, 180

[28] X. Wang, W. S. Liu, X. Lu, P. S. Lee, *J. Mater. Chem.*, 2012, **22**, 23114

[29] X. F. Lu, D. J. Wu, R. Z. Li, Q. Li, S. H. Ye, Y. X. Tong, G. R. Li, *J. Mater. Chem. A*, 2014, **2**, 4706

[30] C. T. Hsu, C. C. Hu, *J. Power Sources*, 2013, **242**, 662

[31] H. Wang, C.M.B. Holt, Z. Li, X. Tan, B.S. Amirkhiz, Z. Xu, B.C. Olsen, T. Stephenson, D. Mitlin, *Nano Res.* 2012, **5**, 605

[32] R. Wang, X. Yan, Sci. Rep. 2014, **4**, 3712

[33] H. Chen, J. Jiang, L. Zhang, T. Qi, D. Xia, H. Wan, *J. Power Sources*, 2014, **248**, 28

[34] R. Ding, L. Qi, M. Jia, H. Wang, *Electrochim. Acta*, 2013, **107**, 494

[35] K. Xu, W. Li, Q. Liu, B. Li, X. Liu, L. An, Z. Chen, R. Zou, J. Hu, *J. Mater. Chem. A*, 2014, **2**, 4795

Supplementary Material

Click here to download Supplementary Material: Supporting information.doc